Chain Dynamics and Relaxation in Amorphous Poly(ethylene terephthalate): A Molecular Dynamics Simulation Study

Sylke U. Boyd and Richard H. Boyd*

Department of Materials Science and Engineering and Department of Chemical and Fuels Engineering, University of Utah, 122 South Central Campus Drive, Salt Lake City, Utah 84112

Received April 16, 2001; Revised Manuscript Received June 21, 2001

ABSTRACT: Chain dynamics in amorphous poly(ethylene terephthalate) have been investigated using molecular dynamics simulations. A previously developed model was adopted with some improvements. Torsional potentials were modified to reflect the results of quantum chemistry calculations and also to accommodate more precise experimental knowledge of the gauche/trans ratio of the glycol ethylene bond. The simulation system size was significantly increased. Autocorrelation functions (ACFs) for the system dipole moment, individual dipole moments, and phenyl ring normals were collected. The temperature range studied corresponds largely to the high temperature merged α and β processes, but the lower end reached the high-temperature limit of experimental dielectric measurements of the β relaxation. ACF relaxation times are in agreement with the position and activation energy of the experimental β peak. Activation energies of conformational transition rates for the three dynamically flexible bond types are very similar to the effective torsional barriers. A disparity between the temperature dependence of relaxation times and conformational transition rates was observed, as well as the development of dynamic heterogeneity with respect to the locations and rates of conformational transitions of individual bonds. Correlations of transitions within a monomeric unit were monitored, and considerable correlation swa found between transitions at the phenyl link and the nearby glycol C−O bond.

Introduction

Poly(ethylene terephthalate) (PET) has been a subject of scientific study for many years. It can be produced with controlled crystallinity, including the nearly completely amorphous state, and provides the base material for applications ranging from fibers to beverage containers and film backings. PET exhibits two major relaxation processes that are associated with the amorphous fraction. The glass transition, conventionally denoted as the α relaxation, occurs at a temperature around 80 °C and is associated with the freezing-out of the cooperative motion of longer chain segments. In semicrystalline specimens, the α relaxation is very noticeably perturbed by the presence of the crystal fraction in that the relaxation region is much broader or diffuse and displaced somewhat to higher temperature. This is a consequence of the natural segment length associated with the underlying motions being appreciable in comparison with the thickness of the amorphous interlayer. The second relaxation is the β relaxation, which occurs below the glass transition and is thus associated with much faster processes. The crystallinity has almost no influence on the location and shape of the β relaxation, which leads to the conclusion that the associated molecular motions must be restricted to short segments of the polymer chain. Both relaxations have been observed via a variety of techniques, including dielectric measurements,[1−5] calorimetric analysis,[6−8] FTIR[9−12] and NMR spectroscopies,[10,13] and dynamic mechanical analysis (DMA).[14−16] Investigations of the relations between the relaxational behavior in the time or frequency domain and sample conditions such as pressure and temperature are the focus of a large number of studies.[1−4,6−12,14−19]

It obviously would be of interest to understand the relaxational behavior of PET in terms of its molecular structure. Eespecially important are the roles played by the different types of constituent bonds in the chain

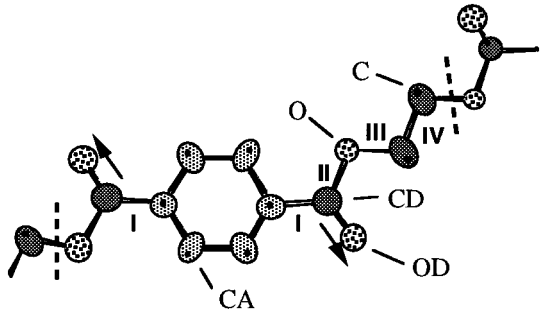

Figure 1. Structure of the monomeric unit. The symbols designate the differently bonded atoms or atom groups: CA = aromatically bonded C/CH group, CD = carboxyl carbon, OD = carboxyl oxygen, C = CH_2 group, O = oxygen. Gray ovals designate centers treated as AUAs containing CA−H or CH_2. The torsion types I, phenyl link; II, ester bond; III, C−O; and IV, C−C in the glycol linkage are indicated.

(Figure 1). For example, the time−temperature location of the α relaxation and the value of T_g must depend on the conformational flexibility of certain bonds and perhaps their ability to undergo locally cooperative or correlated transitions. The β subglass relaxation peak is not well understood at the molecular level. Illers and Breuer[14] reported the resolution of the mechanical isochronal temperature scan β-relaxation peak into three components. This observation was supported by a later study by Armeniades.[20] Both associated the three components with motions of the glycol methylene groups and two conformational states of the carboxyl units attached to one phenyl ring. Three components also appear in the isothermal broad-frequency-band dielectric peak.[4] Sacher observed only two components in a DMA study[1] that were later discussed as being associated with rotational motions of the trans and gauche states of the glycol unit. NMR results of Maxwell et al.[13]

10.1021/ma0106797 CCC: $20.00
Published on Web 09/18/2001

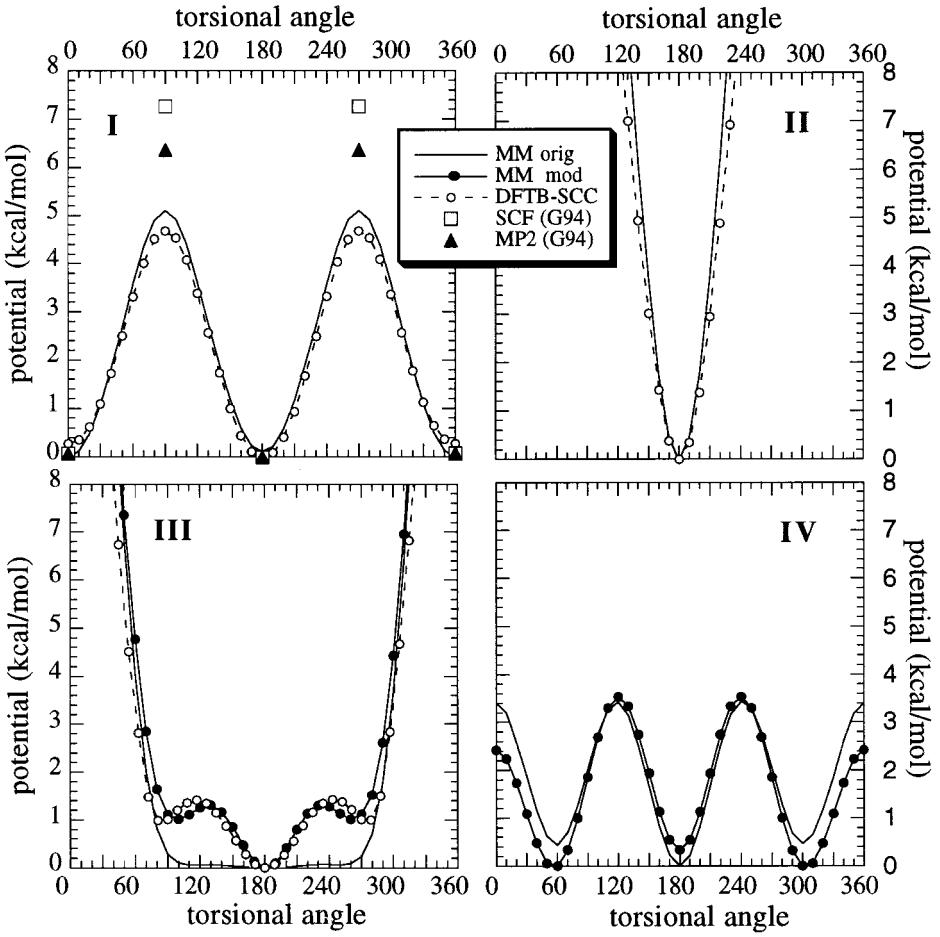

Figure 2. Torsional energy in PET. Included are the original CEM, data from SCC-DFTB, and Gaussian 94 calculations, as well as the modified CEM, if applicable. Note that the plotted lines are the total energy, in contrast to just the explicit torsional energy function in Table 1.

indicate that the phenyl unit, together with the attached carboxyl groups is a major contributor to the β relaxation.

In the present study, molecular dynamics (MD) simulations are used as a tool to gain insight into the processes governing relaxational behavior on a molecular level. In previous work, an energy model or force field (called HBB hereafter for Hedenqvist, Bharadwaj, and Boyd) was developed and successfully applied to MD simulations of the structure and packing of bulk amorphous PET. [21] This basic model is adopted here, but improvements have been made in the force field terms dealing with bond torsions, and a considerably larger simulation system has been invoked.

Simulation Details

The simulation model for PET previously adopted is utilized here.[21] The molecule is represented with a united-atom model, as shown in Figure 1. The hydrogen atoms residing on aromatic carbon atoms (CAs) are contracted into the latter to form a united-atom group with the center displaced outward from the carbon positions, i.e., an anisotropic united-atom (AUA) center.[22] The ethylenic carbon and hydrogen atoms also form an AUA center. Some improvements and verification of the torsional potentials were undertaken as described below.

Modification of the Force Field and Torsional Potentials from Quantum Chemistry. Quantum chemistry (QC) calculations of the torsional potentials for rotation about bond types I−III in Figure 1 were carried out on the model compound dimethyl terephthalate using a density functional theory (DFT) based tight-binding (TB) scheme with self-consistent charge redistribution (DFTB-SCC or, more simply in what follows here, DFT).[23] In addition, calculations of the barrier for bond type I were made using the more numerically intensive but ab initio self-consistent field Hartree−Fock (SCF-HF) method, including geometry optimization, via the Gaussian 94 computational package.[24] The basis set was 6-311G**. Further, electron correlation contributions were estimated using Møller−Plesset second-order perturbation theory (MP-2).[25]

The DFT results for types I−III are shown in Figure 2. The SCF-HF and MP-2 results for type I torsions are also shown there. The comparison of these results with force field parameters to be used in MD simulations is not entirely direct. That is because, in the latter case. an effective torsional barrier is made up not only of the explicit torsional potential expressed as a function of the torsional angle in question but also of contributions from nonbonded interactions, both intra- and intermolecular, and electrostatic interactions. Because the QC computations are carried out on an isolated model molecule, the most reasonable comparison with a force field also is to be made on a molecular fragment. This was accomplished here by means of molecular mechanics (MM) energy calculations on a model molecule as a function of stepwise-fixed values of the torsional angle in question while the energy computed from the complete force field was minimized at each step with respect to all other internal degrees of freedom. An isolated molecule consisting of a PET dimer was used for this purpose.

The dependence of the total energy on the respective torsional angles in the MM calculations is shown in Figure 2. The calculations based on the original HBB force field are labeled as "MM orig". In the case of bond type I, the bond attaching the ester group to the aromatic ring (OD−CD−CA−CA), it can be seen that the DFT results are in good agreement

Table 1. Parameters for the Explicit Torsional Potentials

$$V(\vartheta) = \frac{1}{2}\sum_{i=1}^{2} V_i(1 + a_i \cos b_i \vartheta)$$

	V_1 (kcal/mol)	a_1	b_1	V_2 (kcal/mol)	a_2	b_2
CA−CD−O−C (II)	14.0	−1	2	4.0	1	1
OD−CD−CA−CA (I)	2.5	−1	2	0.0	0	0
CA−CA−CA−CD	13.0	−1	2	0.0	0	0
CA−CA−CA−CA	26.0	−1	2	0.0	0	0
CD−O−C−C (III)	0.8	−1	4	1	−1	2
O−C−C−O (IV)	3.2	1	3	−0.8	−1	1

Table 2. Trans Fraction at the O−C−C−O Ethylenic Bond in Bulk PET

T (K)	trans fraction (%)
650	22.8
500	20.7
400	15.9
300	15.2
250	14.4
200	14.4

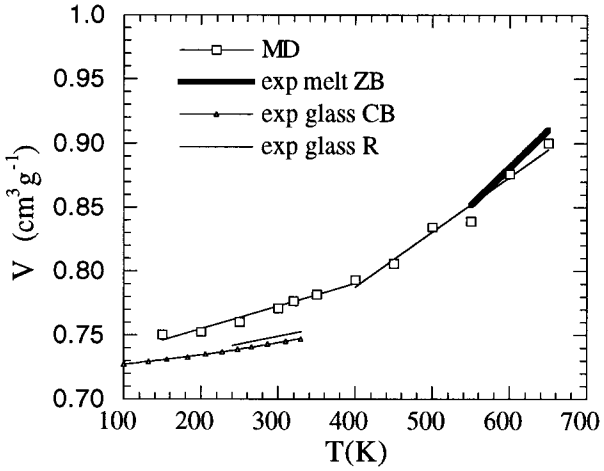

Figure 3. Specific volume versus temperature. The glass transition temperature T_g of the model can be located at 400 K. The experimental references are Reddish[36] and Coburn and Boyd.[2]

with the MM results using the original force field. The ab initio SCF-HF results are somewhat higher than the DFT ones, but when the MP-2 correlation is introduced, the energy is lowered. In view of the uncertainties and the general level of agreement, no modification of the HBB parameters was made for this torsion. The DFT results for the ester group planarity, bond type II, are in good agreement with the MM results. Effectively, this bond does not contribute to relaxation because of the high barrier. No adjustment was made to the original force field. In the case of the C−O bond in the glycol moiety, however, there are significant differences between the DFT results and the HBB force field. As explained in detail previously,[21] in order to reproduce the experimental dipole moment ratio of PET, it is necessary that the trans conformation of the CD−O−C−C bond be significantly favored energetically over gauche. The HBB force field accomplished this, but as can be seen in Figure 2, the effective potential is a broad minimum centered on the trans state with a very high barrier at the cis planar position. The DFT results also find a very high barrier at cis planar but suggest more structure at the gauche positions. This structure has now been incorporated into the force field via the parameters listed in Table 1. The result can be seen in Figure 2 as the modified MM curve.

Finally, some QC calculations were carried out concerning the O−C−C−O torsion. These were restricted for computational tractability to the somewhat structurally inadequate model molecule 1,2-ethylenediol diformate. It was found that both the DFT and SCF-HF methods predict that the energy of the gauche state is somewhat higher than that of the trans state. Experimental evidence concerning the trans fraction, however, indicates otherwise. Vibrational spectroscopy has indicated lower values (trans fraction of 5−25%) than consistent with equal energies.[26−31] Recent NMR results have confirmed values in this lower range.[32] The HBB simulation invoked an O−C−C−O potential that favored the gauche conformation but resulted in this fraction being found from the simulations as ∼40%. Further, there appears to be no way to lower the trans fraction significantly except by parametrization of the O−C−C−O bond potential. Consequently, the HBB potential was modified empirically to favor gauche more strongly, as shown in Figure 2. The parameter values are given in Table 1. The trans fractions found from MD sampling of the bulk system at a number of temperatures are shown in Table 2, where it is seen that the fraction is now about 15% over most of the range.

Simulation System. In the present study a significantly larger system than the previous one is utilized. Eight polymer chains with 20 monomers each were inserted in a cubic box with periodic boundary conditions (in comparison with a single chain of 60 monomers previously). This results in 2240 force centers. All energy parameters, with the exception of the modified torsional parameters discussed above and listed in Table 1, are given and described in detail in Table 1 of Hedenqvist, Bharadwaj, and Boyd.[21]

The initial system was equilibrated for several nanoseconds under a constant pressure of 1 atm and a temperature of 650 K. Other lower temperatures were reached by stepwise cooling under *NPT* dynamics. For *NPT* dynamics, the Martyna et al. formulations of the thermostat[33] and the barostat[34] were used, along with a velocity Verlet integrator. The statistical data sampling at each temperature was performed under *NVT* conditions with the above thermostat but with an explicit reversible integrator that permitted multiple time steps.[35] For the valence force interactions (stretch, bend, and torsion), a time step of 1 fs was used, and for the nonbonded interactions, 2 fs was used. Although the separation of time scales is not dramatic, it effectively resulted in a near halving of the computation times. The *NVT* sampling runs at each temperature were 2 ns each and were preceded by an initial equilibration in the *NPT* ensemble of 0.5 ns.

Structural Results

Volume−Temperature Behavior. Specific volumes determined from time-averaged system volumes during the *NPT* equilibration at each temperature are shown in Figure 3. Also shown are experimental results for the glass[2,36] and melt.[37] The MD results are very similar to those found previously.[21] The MD melt values agree well with experimental results. The glass volumes are somewhat higher than experiment (2−3%). This circumstance might well result from the difficulty in MD simulation in achieving the densification for a complex chemical structure that is obtained much more slowly experimentally. The MD results show a break in slope indicative of a volumetric glass temperature. The straight line segments were arbitrarily fit to the points for 400 K and below and to the points for 400 K and above. On this basis, the MD volumetric glass temperature appears to be slightly over 400 K. This compares to 350 K determined experimentally. The upward displacement of the MD T_g is again an indication of the effect of short MD equilibration times in comparison with those for experiment.[38]

Effective Potentials from Populations. At higher temperatures, in the melt where θ-solvent conditions are presumed to prevail, the populations of the torsional angles of the various bond types should reflect the

energy parameters in the force field that result in the effective torsional potentials and are thus to some degree a validation of the results of the force field parameters chosen. At lower temperatures, at the onset of vitrification, the conformational populations might no longer be in equilibrium, i.e., they might be becoming "frozen-in", so they become diagnostic of glass formation. Thus, it is appropriate to derive effective torsional potentials from torsional angle populations as a function of temperature. This is accomplished through the Boltzmann relation as

$$V(\varphi) = -k_B T[\ln p(\varphi) + \ln Q] \quad (1)$$

where $V(\phi)$ is the derived effective potential, $p(\phi)$ is the fractional MD-sampled torsional angle population, and Q is the partition function. The latter is conveniently taken to zero the potential at the minimum value. The effective potentials thus determined for the three conformationally flexible bond types (I CA−CD, III C−O, and IV C−C, Figure 1) are shown in Figure 4. Also shown are the molecular-mechanics-derived potential curves of Figure 2 for the modified force field. It can be seen that the effective potential points for temperatures of 400 K (near the MD volumetric T_g) and above are clustered tightly together, indicating equilibrated torsional populations. Further, these points mimic the molecular mechanics version of the effective barriers rather well. In the case of the type III C−O bond, the gauche minima are not as well defined as in the MM effective potential. Because the gauche minimum is a very shallow one, this could well be the result of torsional oscillations obscuring it. Below 400 K, however, the populations near the barriers are greater than expected, and thus, the effective potential points are lower. This is a result of the freezing-in of conformational populations characteristic of a higher temperature, an effect noticed before in simulations and attributed to nonergodicity.[39]

Mutual Orientation of Phenyl Rings. In the earlier work, structural characterization via various site−site radial distribution functions was carried out.[21] This is not repeated here. However, the orientation of pairs of phenyl rings with respect to each other was not undertaken previously and is of some interest. It was explored here by sampling the angle, θ, formed by the vectors normal to the rings. Because the rings are somewhat vibrationally deformed, in MD, a ring normal is defined as the sum of the three vector product combinations of the three ring diagonal vectors. The results can be expressed in terms of a P_2 orientation function given by

$$f_\vartheta = \frac{1}{2}(3\langle\cos^2\vartheta\rangle - 1) \quad (2)$$

where the brackets indicate a sampling average over an ensemble snapshot and over time as expressed by a number of ensemble frames. Because the complete system ensemble is likely to mask any nearby correlations, the function was also computed over two spheres of limited radii, 4.5 and 7 Å. The average interchain spacing in amorphous PET was found previously from radial distribution function analysis to be ~5 Å.[21] The phenyl−phenyl orientation results are shown in Figure 5. Because the orientation function has a value of 0 for a random distribution, 1 for perfect parallel alignment, and $-1/2$ for perfect orthogonality, it is apparent that, as expected, there is no alignment over the system. Over the restricted spheres, there is a noticeable but very slight parallel orientation.

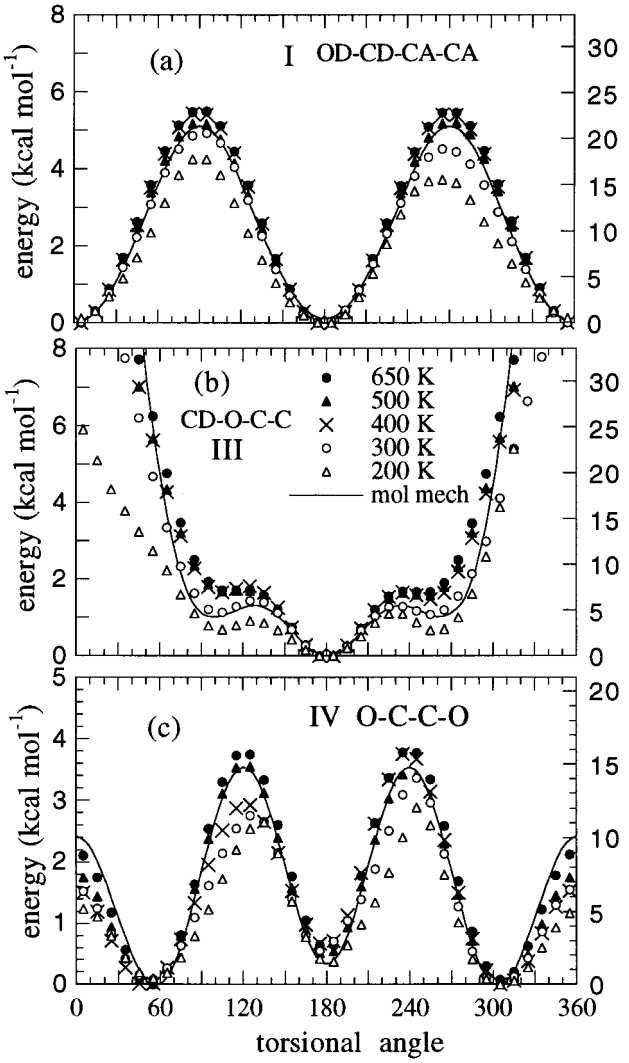

Figure 4. Torsional potentials derived from population analysis. (a) phenyl linkage I, (b) C−O bond in glycol linkage III, and (c) C−C bond in glycol linkage IV. The symbols indicate the temperatures at which the samples were taken: ●, 650 K; ▲, 500 K; ◆, 400 K; ○, 300 K; and △, 200 K. The solid line indicates the relaxed potential from molecular mechanics calculations as described in the Simulation Details section. The right-hand ordinate labels are in kJ mol^{-1}.

Dynamical Results

Autocorrelation Functions. The dynamical behavior of a property of the simulation system is conveniently summarized in terms of an autocorrelation function (ACF). For comparisons with experimental dielectric results dipolar ACFs were determined. The system moment at time t, $\bar{M}(t)$, is constructed from the sum of the individual ester group dipole moments, $\bar{\mu}_i(t)$

$$\bar{M}(t) = \sum_i \bar{\mu}_i(t) \quad (3)$$

The dielectric relaxation strength is determined by equilibrium statistical mechanical value of $\langle\bar{M}(0)\cdot\bar{M}(0)\rangle$

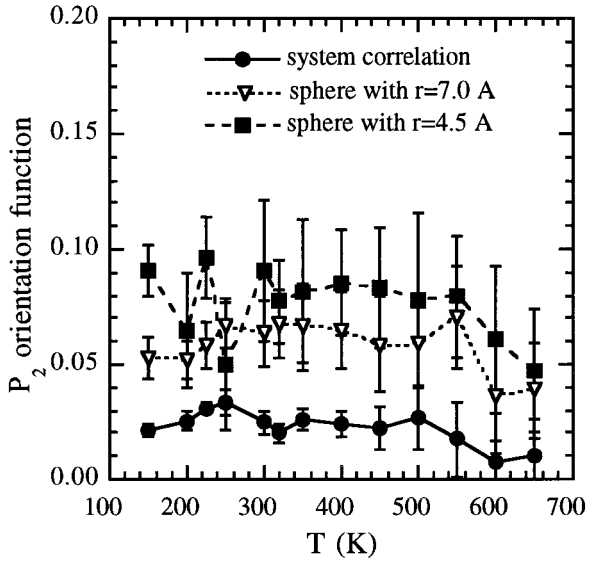

Figure 5. Correlation of ring normal vectors according to a P_2 orientation function as a function of temperature. The overall system correlation and the short-range correlation for two radii are shown.

and is related to the Kirkwood−Onsager expression[40] for the dipolar correlation factor, g, by

$$g = \langle \bar{M}(0)\cdot\bar{M}(0)\rangle / N\bar{\mu}^2 \tag{4}$$

where μ is the magnitude of the ester group moment and N is the number of dipoles in the volume defining the system moment. It was previously demonstrated, and reconfirmed here, that the simulation gives a good accounting for the experimental g factor thorough eq 4.[21] In the present work on chain dynamics, time dependence is emphasized. The connection to experiment is established via the normalized system moment ACF defined as

$$f_M(t) = \frac{\langle \bar{M}(0)\cdot\bar{M}(t)\rangle}{\langle \bar{M}(0)^2\rangle} \tag{5}$$

where the brackets indicate averages over multiple starting points $t = 0$. The function is related experimentally to the normalized time-dependent retarded dielectric constant $\epsilon(t)$ by

$$f_M(t) = \frac{\epsilon(\infty) - \epsilon(t)}{\epsilon(\infty) - \epsilon(0)} \tag{6}$$

In the simulation sampling carried out here, individual moments, $\bar{\mu}_i(t)$, used to construct the system moment via eq 3 are taken as unit vectors along the carbonyl CD−OD bond.[41,42]

Another dipolar ACF that can be considered is one based solely on the individual dipoles

$$f_\mu(t) = \langle \bar{\mu}_i(0)\cdot\bar{\mu}_i(t)\rangle / \mu^2 \tag{7}$$

where the brackets also include averaging over all dipoles. This function does not contain the cross terms $\bar{\mu}_i(0)\cdot\bar{\mu}_j(t)$ that arise in eq 5 from the sum in eq 3. Although this function is not directly related to the experimental dielectric results, it does have the advantage of being much less statistically noisy than the system moment ACF, and it is still related to the

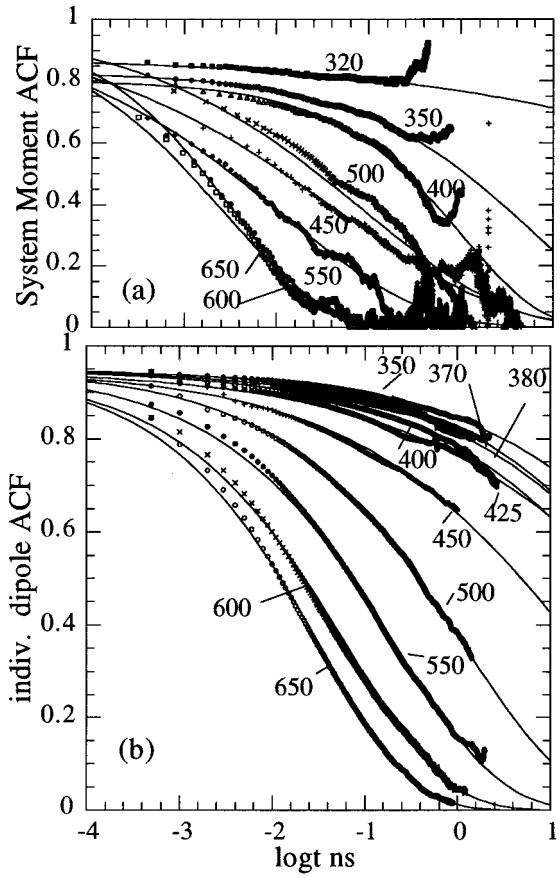

Figure 6. Dipolar autocorrelation functions versus log t at the temperatures (in Kelvin) indicated. Upper panel is the system moment and the lower panel is for individual moments. The curves are KWW equation fits to the MD data. In the fits for the individual moments, a premultplier of 0.95 in eq 10 was used and for the system moments premultipliers of 0.88 at 320 K, 0.83 at 350 K, and 0.80 at 400 K were used.

average local dipolar relaxation. In addition, experience has shown,[39,43] and it has been confirmed here, that $f_\mu(t)$ tends to closely mimic the torsional angle ACF. The latter ACF is defined[44] as

$$f_\varphi(t) = \frac{\langle \cos\varphi(0)\cos\varphi(t)\rangle - \langle\cos\varphi(0)\rangle^2}{\langle\cos\varphi^2(0)\rangle - \langle\cos\varphi(0)\rangle^2} \tag{8}$$

Finally, it is useful to directly monitor the relaxation of the phenyl rings considered as a rigid unit. This was done by construction of an ACF based on a unit vector normal, $\bar{n}$, to the ring or

$$f_{\text{ring-n}}(t) = \langle \bar{n}(0)\cdot\bar{n}(t)\rangle \tag{9}$$

Comparison with Experimental Dielectric Measurements. Simulation results for both the system moment and individual dipole functions, $f_M(t)$ and $f_\mu(t)$, respectively, are shown at a number of temperatures in Figure 6. It is apparent, as suggested above, that the system moment functions are much noisier than individual dipolar functions. To extract descriptors for comparison with experimental results, both sets of results were fit to the Kohlrausch−Williams−Watt (KWW) stretched exponential function[45]

$$f_{\text{KWW}}(t) = \exp(-t/\tau)^\beta \tag{10}$$

The solid curves in Figure 6 are these fits. In ac-

complishing the fitting, as has been observed in other systems,[39] a noticeable initial fast decay is apparent. It appears to be unrelated to the ensuing relaxation processes and is attributed to dipolar motions occasioned purely by torsional oscillations. In the individual dipolar case, it was factored out by using a premultiplier in eq 8 equal to 0.95. The effect seems even greater for the system moment, but it was invoked only at the lower temperatures. The premultipliers used are given with Figure 6. A caveat is issued here. At the lower temperatures, relaxation is far from complete, a consequence of the inevitable limit on MD trajectory lengths imposed by practical computation times. Nevertheless, the fits are good over the limited range and allow relaxation times that are decades larger than the run lengths to be determined. However, there is no guarantee the real physical behavior would continue to follow that particular KWW form at longer times. In addition, the combination of relaxation times and β parameter values determined becomes increasingly less unique in a numerical regression sense as the extent of observed relaxation decreases.

To facilitate comparison with experiment, the resulting KWW relaxation times were converted to frequency-domain frequencies of the maximum dielectric loss factor, f_{max}. This conversion utilizes the fact that the maximum in the loss component in the Fourier-transformed KWW function occurs very close to that given by $2\pi f_{max} = 1/\tau_{KWW}$. In Figure 7a, a loss map of log f_{max} vs reciprocal temperature compares the MD and experimental results. Also shown in Figure 7b are the companion β parameters.

The experimental results displayed in Figure 7 are for both the α glass transition region and the β subglass relaxation process.[2−4] The α region is extrapolated to higher temperature by means of a Vogel−Fulcher (VF) equation[46]

$$\log f_{max} = A - B/(T - T_0) \qquad (11)$$

fit to the combined α-region experimental data sets[2,3] shown. The VF parameters found are given in the figure legend. The experimental KWW β parameters shown in Figure 7b were determined directly from fits of time-domain dielectric constant measurements.[47] It is apparent that the experimental α and β processes merge with increasing temperature. In fact, the elucidation of the details of this merging was the object of a Hoffmann, Kremer, and Fischer study.[3] Stated conversely, in the high-temperature melt rapid chain dynamics result in a unified process. Local conformational transitions (bond rotations) are so frequent that little cooperativity is required to occur to effect complete relaxation. As the temperature is decreased, the elementary conformational transitions become infrequent enough that complete relaxation is accomplished via some recipe of cooperative events involving spatial scales on the order of several persistence lengths. The elementary conformational jumps maintain an Arrhenius temperature dependence, but the more cooperative motions have a much stronger temperature behavior. As a result, a bifurcation occurs as temperature decreases into a faster branch involving partial relaxation via localized conformational transitions and a slower more temperature-dependent branch that effects more complete relaxation via a cooperative series of transitions.

It is apparent in Figure 7 that the simulation domain is that of the unified processes in the high-temperature

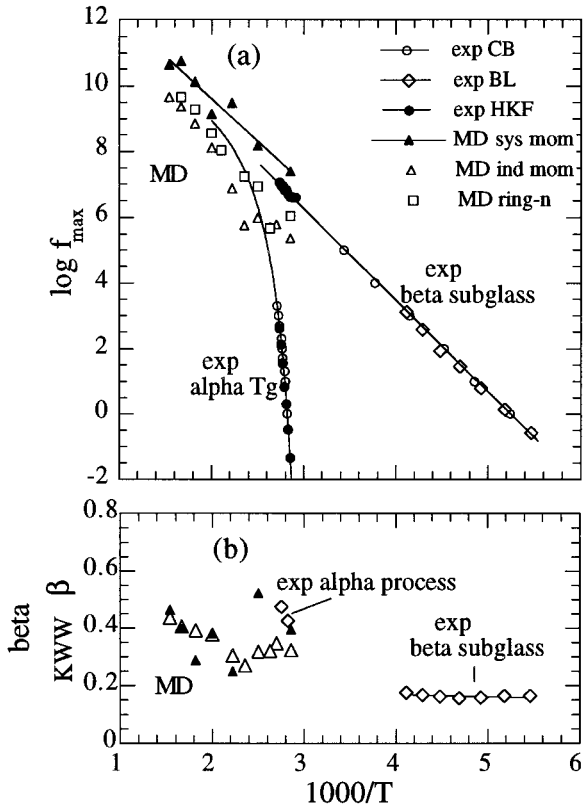

Figure 7. Upper panel: Dielectric loss map for PET where the location of the loss peak in the frequency domain (log f_{max}) is plotted vs the reciprocal temperature. The open circles (CB) are experimental data from ref 2; open diamonds (BL) are from ref 4; filled circles (HKF) are from ref 3. The solid line through the combined β-region data is a linear regression that gives an activation energy of 12.9 kcal mol^{-1}. The curve through the combined α-region data and extrapolated to higher temperature is a Vogel−Fulcher equation (eq 11) regression with parameters $A = 11.02$, $B = 374.6$, and $T_0 = 320.2$. The filled triangles are derived from MD simulation KWW relaxation times for the system dipole moment; the linear regression shown gives an activation energy of 11.8 kcal mol^{-1}. The open triangles are for the individual dipole moments, and the open squares are for the phenyl ring normal ACF. Lower panel: KWW β width parameters vs reciprocal temperature for both experiment and simulation with the same symbols as the upper panel. The ring normal function values are similar to the individual dipolar ones and are not shown for clarity in the plot.

melt and of the approach to bifurcation. The system moments, which are directly related to the experimental dipolar process, follow the implied experimental behavior well. The activation energy in the range of the MD simulations is the same as that of the experimental β branch (12 kcal mol^{-1}). The KWW β parameters from the simulation in Figure 7b are also consistent with the high-temperature experimental values. Thus, because, as commented above, the experimental g factor is reproduced, the simulation is successful in reproducing the both the strength and dynamic features of short-time, higher-temperature experimental dielectric relaxation.

The individual dipole moments relax noticeably more slowly than the system moment. This not surprising, perhaps, as there is considerable equilibrium dipolar correlation. The experimental Kirkwood−Onsager g factor is considerably less than unity.[2,21] The latter situation can be rationalized in terms of rotational isomeric state (RIS) calculations of the dipole moment

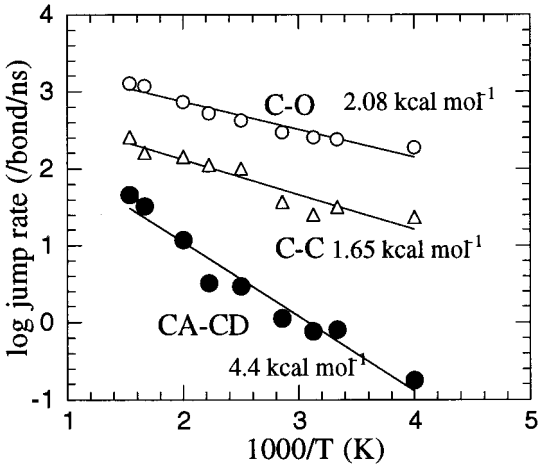

Figure 8. Temperature dependence of conformational transition rates. The logarithm of the transition rate is plotted vs the reciprocal temperature for the three indicated bond types. Activation energies computed from the linear regressions shown are displayed.

ratio, which were utilized in the formulation of the force field parameters.[21] Thus the more rapid loss of correlation accompanying the system moment ACF decay could well be assisted by the large contribution of interdipolar terms as opposed to the purely self-correlation terms in the individual dipolar ACF.

Interpretation of Chain Dynamics

Conformational Transition Rates. With reasonable correspondence to experiment established, it is now appropriate to discuss what the implications of the simulations for the details of the chain dynamics. One of the questions of interest concerns the relative roles or importance of conformational transitions in the three types of dynamically flexible bonds in the chain, i.e., the −CA−CD− bond connection of the phenyl ring to the ester group, the −O−C− glycol linkage, and the −C−C− ethylenic bond. Conformational transition rates for the three bond types are given in the form of an Arrhenius plot in Figure 8. The transitions were counted on the basis of a given bond having visited a minimum in the torsional potential (CA−CD, 0°, 180°; O−C, ±90°, 180°; C−C, ±60°, 180°) within ±5° tolerance and, at a later time, having visited another minima within the same tolerance. The activation energies determined from the slopes of the curves are also indicated in the figure. These reflect the torsional potentials (Figures 2 and 4) in that they are near the barrier values. The value for the CA−CD bond, 4.4 kcal mol^{-1}, compares to ∼5 kcal mol^{-1} in Figures 2 and 4. The rate for the C−C bond is dominated by the lower of the two barriers, i.e., the gauche-to-gauche barrieratwith 1.7 kcal mol^{-1} in Figure 8 compared to a range about this same value in Figure 4. For the C−O bond, the value of 2.1 kcal mol^{-1} in Figure 8 compares to a range of 1.5−1.9 kcal mol^{-1} in Figure 4. It is interesting to note that the order of transition rates does not follow the activation energy sequence in that the C−O bond transition rates are higher than those for the C−C bond. The consequently higher value of the preexponential factor for the C−O bond is probably the result of the shape of its torsional potential. The C−O bond has a very shallow broad minimum at the ±90° state, with a small maximum separating this state from the one at 180°. Such a potential would be expected to give increased weight to the 180° state compared to one with a deeper minimum.

Thus, the circumstance prevails that the activation energy for the decay of the dipolar ACF (∼12 kcal mol^{-1}) is considerably higher than those for the conformational transition rates, the latter directly reflecting the torsional barriers. This behavior seems to be general. There are three other systems for which similar simulations of chain dynamics have been made and are available for comparison. These are polyethylene (PE),[39,43] polybutadiene (PBD),[48] and Vectra-type aromatic copolyester liquid crystalline polymers (LCPs).[49] The first two polymers have very dynamically flexible chains and low glass temperatures.[50−52] In the LCPs, the relaxation processes occur at considerably higher temperature. In all three polymers, the conformational transition rates have Arrhenius temperature dependence with activation energies near the barrier values in the population-sampled torsional potentials. The ACF KWW relaxation time−temperature behavior is more complex. In PE at high temperature, the ACF relaxation time−temperature dependence approaches that of the transition rates, but as the temperature is lowered, the ACF behavior diverges and then becomes Arrhenius-like but with a much higher activation energy. PBD exhibits behavior similar to this that is somewhat complicated by the presence of two kinds of flexible bonds and the possibility of a cis or trans double-bond configuration. In the LCP, the ACF relaxation time behavior is Arrhenius over the temperature range available to simulation but with an activation energy that is much higher than that for the transition rates. It is the latter situation that prevails here for PET.

Spatial Dynamic Heterogeneity. The disparity between the temperature dependence of the transition rates and ACF relaxation times in PE,[39,43] PBD,[48] and the LCP[49] has been associated with the onset of dynamic heterogeneity as temperature is lowered. At high temperature under ergodic conditions, the bonds of a given type are equivalent in their dynamic behavior, including transition rates, over a sufficiently long time interval. However, as temperature is lowered toward vitrification, the bonds become nonequivalent. Some exhibit high transition rates and some have much lower ones. This change reflects the development of nonequivalent locations in the glass associated with specific conformational sequences and differences in packing. Because the ACF is an average over all bonds, its behavior largely reflects the many bonds with only a few transitions. The reason the overall conformational transition rate maintains the high-temperature Arrhenius behavior to low temperature is not as clear. It appears to be related to the phenomenon that the lifetimes of occupation of a given place along the effective torsional potential increase greatly as vitrification is approached.[39,43] These lifetimes are long enough that, in a transition state context, transitions are initiated from points along the barrier rather than from a bond oscillating about the torsional minimum. Those few bonds nearer the top of the barrier find very low barriers and consequently exhibit high transition rates.

Spatial heterogeneity in the conformational transition rates is found here in PET as well and is illustrated in Figure 9. The percentage of the total transitions of a given bond type occurring at a specific bond over a simulation sampling are plotted versus the individual bond locations as described by a sequential numerical

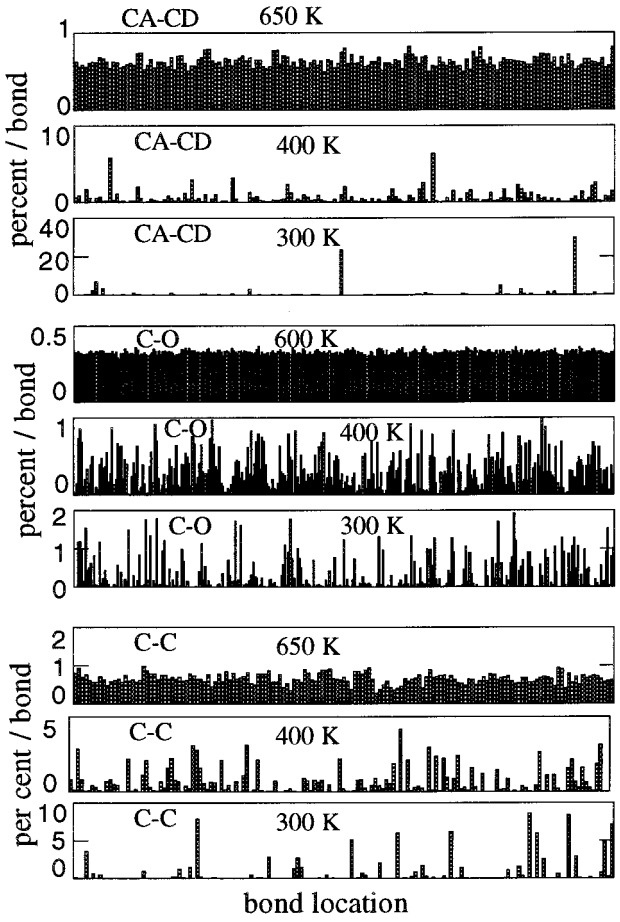

Figure 9. Spatial heterogeneity in the conformational transition rates. The percentages of conformational transitions occurring at each bond are plotted against location (a numerical index of the bond position along the chain). Results are shown at three temperatures for each of the three bond types CA−CD, C−O, and C−C.

index that advances with the position along the chain and from chain to chain. Results are displayed for each of the three bond types at three temperatures, corresponding to a high-temperature melt (600 or 650 K), an intermediate temperature where relaxation is slow (400 K), and a low temperature (300 K) where transitions are observed but relaxation is too slow for reliable ACF relaxation times to be determined. The change from a random distribution that has approached uniformity at high temperature to a distribution at low temperature in which a few high rate spikes appear is evident.

Correlation of Transitions. An important issue in chain dynamics is the question of the degree to which conformational transitions are correlated. In this context, correlated means that pairs of transitions often occur in a concerted manner. One transition occurs and is followed preferentially by another transition at another bond. In PE, for example, correlated transitions occur to a noticeable extent in the high-temperature melt,[43,53] and in the glass, almost all relaxation involves correlated transitions.[39] This is the result of the obvious problem that an isolated bond rotation requires considerable alleviation of strain by displacement of the torsional angles of other nearby bonds and of other chains. This alleviation of strain becomes more difficult at lower temperature and correlated transitions are a more efficient way of effecting conformational transitions.

In PET, we focus on the interactions between the three types of conformational flexible bonds within a monomeric unit. The group of bonds considered is the sequence consisting of a phenyl group link, which is the CA−CD bond; the O−C bond following this; the C−C bond following; the C−O following and finally, the next CA−CD phenyl link. A procedure used previously for recording correlations was invoked.[43] The transitional state of each bond is investigated at each time step. If it changes according to the same criteria used for counting transitions above, this is noted. Then, in each time step, the conformational state of each of the bonds in the "window" of the above monomeric sequence is scanned (including the bond on which attention is being focused). When the first change in one of the states occurs, a "correlated" transition is recorded. Although this is a temporal sequence judgment, no time limit is invoked in the classification.[43] In addition, the results have to be compared to random expectation.

The results of the correlation classification are given in Figures 10−12. Because the rates of conformational transition are quite different for the three types of bonds (see Figure 8), the probabilities of a transition following a jump at a given bond type are not directly meaningful. However, a probability can be compared with what would have been observed if there were no actual correlation, i.e., if the transitions had occurred at random with respect to type. Such a comparison can be accomplished by utilizing the rates of individual transitions (Figure 8). For example, the rates of transition, $\dot{R}$, can be used to formulate the random probability expectation for the next jump of type C−C as

$$p_{\text{random}}(\text{C}-\text{C}) = \frac{\dot{R}_{\text{C}-\text{C}}}{\dot{R}_{\text{C}-\text{C}} + 2\dot{R}_{\text{C}-\text{O}} + 2\dot{R}_{\text{CA}-\text{CD}}} \quad (12)$$

In Figures 10−12, random probabilities formulated in this manner are shown in comparison with sampled values derived from MD sampling.

For the C−O bond, the upper panel of Figure 10 indicates that, although the self-correlation and jumps at the other C−O bond are random at high temperature, as temperature decreases, self-correlation becomes more and more prevalent. This behavior is found in other systems[43,54] and is associated with the development of nonergodicity and spatial heterogeneity, as discussed above. The correlation of the C−O bond with ensuing CA−CD phenyl link transitions, as seen in the middle panel, favors the nearby link over the farther one. This correlation increases with temperature, an effect no doubt due to the relatively stronger temperature dependence of transitions of the phenyl link bond (Figure 8). The C−C bond, as seen in the lower panel, is uncorrelated with the C−O bond.

The CA−CD phenyl link shows, as seen in the upper panel of Figure 11, very significant positive correlation with the nearby C−O bond and negative correlation with the farther one, as was seen for the reverse situation in Figure 10. Self-correlation, in the middle panel, prevails strongly over correlation with the phenyl at the other end of the monomeric moiety. Correlation with the C−C bond (lower panel) appears to be absent.

The C−C bond (Figure 12, upper panel) exhibits an expected and strong self-correlation behavior. Coincident with the high-temperature decline in the self-correlation is an increase in C−O bond correlation toward random behavior. For the CA−CD phenyl link

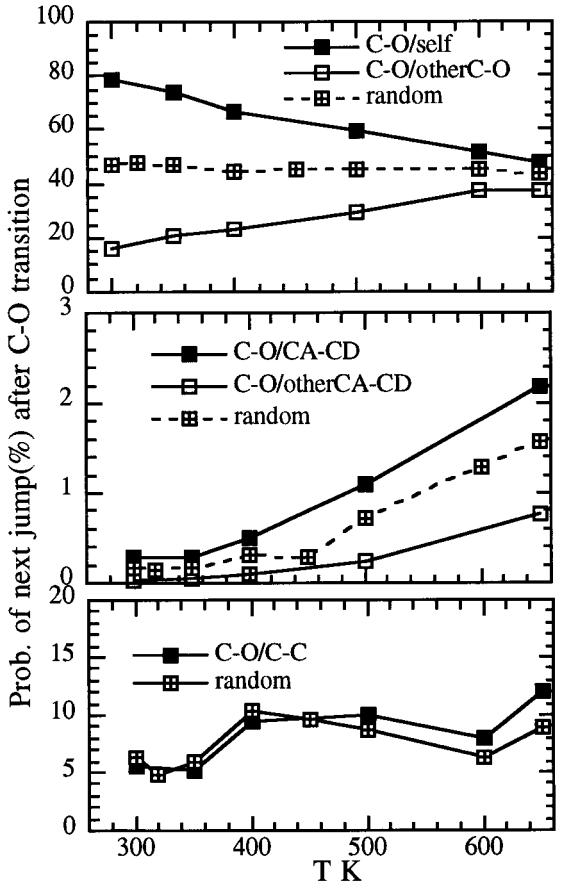

Figure 10. Transition correlations at the C−O bond in terms of the probability (%), as determined by MD sampling, that a transition at the bonds indicated within a single monomeric unit follows a transition at the C−O bond. The upper panel is for the self-correlation of the C−O bond (returns to its original state before another transition occurs) and for the correlation with the other C−O bond in the unit. Also shown is the result, based on measured rates of single transitions, that would have been found if the indicated transition correlations occurred at random. The middle panel shows the results for the C−O transition being followed by a transition at the nearby phenyl link (CA−CD) bond and the other farther away CA−CD bond in the unit sequence. The lower panel shows the correlation with the C−C glycol bond.

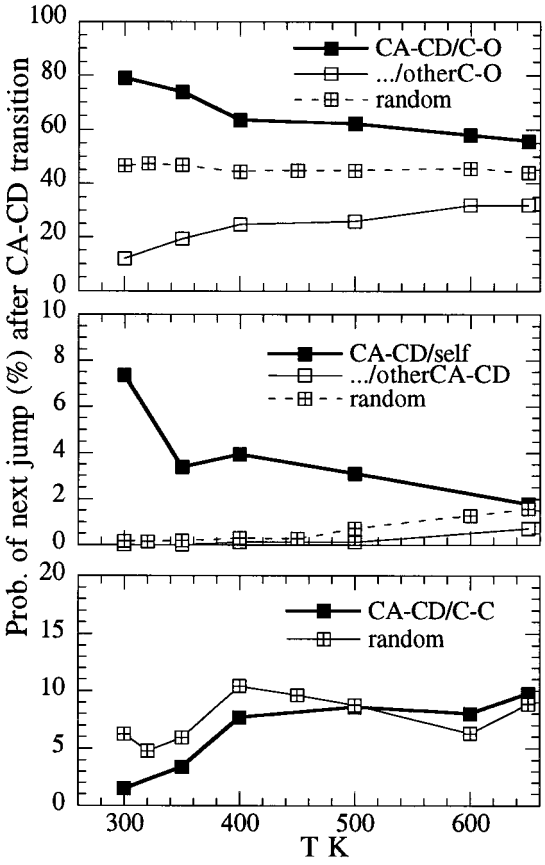

Figure 11. Transition correlations at the CA−CD phenyl link. The upper panel is for the correlation with the nearby C−O and the other farther away C−O bond in the unit. The middle panel shows the self-correlation of the CA−CD bond and the other CD−CA bond at the other end of the unit. The lower panel is for the correlation with the glycol C−C bond. All of the panels show the results that would have been obtained if the correlation were random.

(lower panel), the correlation is seen to be negative. However, the probabilities involved are quite small.

The overall conclusion to be drawn is that the correlation between jumps at the phenyl link and the nearby C−O bond is considerable.

Phenyl Group Motion vs Ester Dipole Motion. Because the ester group is separately effectively dynamically rigid, an individual ester group dipole can be considered to be directly appended to the CA−CD bond at the CD atom. Likewise, the CD atom can also be considered as attached to the O atom of the O−C bond. Dipolar reorientation is directly effected by a conformational transition at the CA−CD bond, as opposed to collateral dipolar excursions from conformational transitions at other nearby bonds. The question arises as to the degree to which the phenyl ring undergoes motion in comparison with ester dipole motion when a CA−CD transition occurs. It could be imagined that, because the phenyl group is bulky in comparison with the dynamically flexible connecting glycol linkage, the angular excursion of the ester dipole could tend to be greater than that of the phenyl ring. An indicator of this could be in the ACF based on the normal to the phenyl ring formulated in eq 9. It is seen in Figure 7 that the KWW relaxation times for the phenyl normal are very similar to those for the individual dipole relaxation (eq 7). Thus it appears that, overall, including the statistical effects of all transition types, the rate of phenyl ring reorientation is very comparable to the rate of reorientation experienced by the ester dipole.

Bond Types and β Relaxation. A question related to the one immediately above has to do with the relative importance of the three bond types in the relaxation rate of the ester dipole, especially in the β-relaxation region. The transition rate is least at the phenyl link, highest at the C−O bond, and intermediate at the C−C bond. From an *equilibrium* point of view (as concluded from RIS model calculations[21]), the relaxation strength is very sensitive to the relative cis/trans population across the phenyl ring, as well as to the C−O bond gauche/trans population but much less so to the C−C gauche/trans bond population. Dynamically, it is interesting to compare the effects of freezing these populations. The effects on the individual dipolar ACF of imposing a very high barrier on each of the bond types are shown in Figure 13. It can be seen that, indeed, the dynamic flexibility of all three bond types plays an important role in the relaxation and that the order of sensitivity is consistent with the effects on equilibrium relaxation strength. This has a bearing on the β-relaxation mechanism.

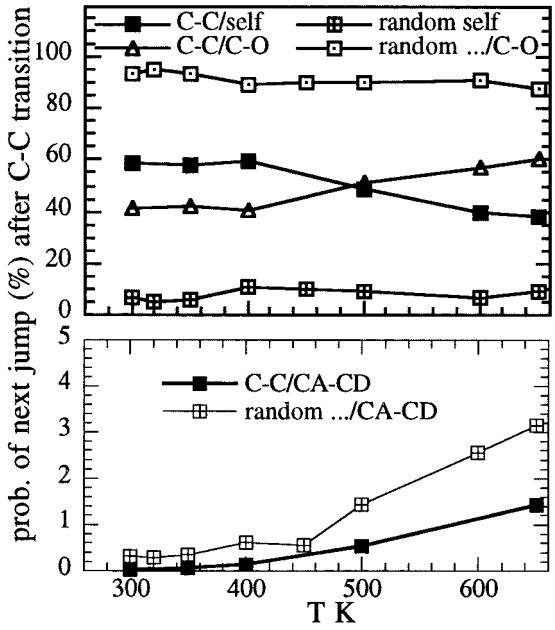

Figure 12. Transition correlations at the C−C glycol link. The upper panel is for self-correlation and for correlation with the C−O bond. The results that would have been obtained if the correlations were random are shown for both types. The lower panel shows the correlation with the phenyl link CA−CD bond.

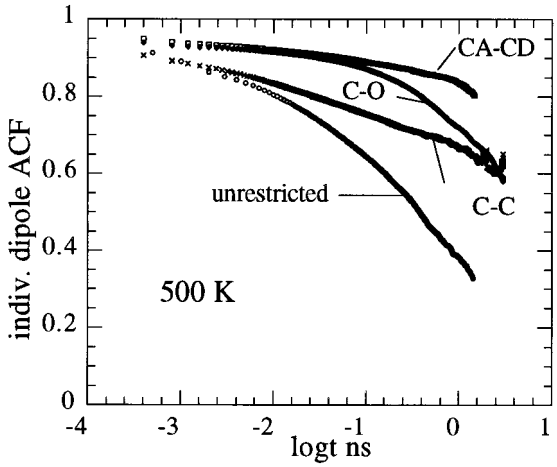

Figure 13. Effect of constraining motion at each of the bond types on the individual dipolar ACF. An artificially high barrier was invoked at the indicated bond types while the ACF was determined.

As noted in the Introduction, there is experimental evidence that that the β relaxation is complex in that it appears to consist, at much lower temperatures and hence with possibilty of higher resolution than accessible to MD simulation, of overlapping components. It would seem reasonable to conjecture that the components could be associated with each of the three bond types. The results of this work are consistent with such a conclusion. Even at 500 K (Figure 13), if the least flexible type (the phenyl link CA−CD bond) does not participate, the extent of relaxation at long times is quite small. Further, as discussed, a correlation between the phenyl link and C−O bond transitions exists at low temperature. It does not seem possible that the β relaxation does not involve conformational transitions in this type as well as in the other two higher-rate types of transition bonds.

It is also of note that, even though the relaxation region available to simulation in the present study (see loss map Figure 7) is largely in the merged region, the activation energy has already taken the Arrhenius value characteristic of the β relaxation. This would argue that the bond rearrangements in the simulation accessed region are typical of the β region.

Acknowledgment. S.U.B. is indebted to the Deutsche Forschungsgemeinshaft (DFG) for a fellowship. We are grateful to the National Science Foundation, Polymers Program, for financial support. The use of computational facilities at the University of Utah Center for High Performance Computing and the Technical University Paderborn is also gratefully acknowledged.

References and Notes

(1) Sacher, E. *J. Polym. Sci. A-2* **1968**, *6*, 1935.
(2) Coburn, J. C.; Boyd R. H. *Macromolecules* **1986**, *19*, 2238.
(3) Hofmann, A.; Kremer, F.; Fischer, E. W. *Physica A* **1993**, *201*, 106.
(4) Boyd, R. H.; Liu, F. in *Dielectric Spectroscopy of Polymeric Materials*; Runt. J. P., Fitzgerald, J. J., Eds.; American Chemical Society: Washington, D.C., 1997.
(5) Canadas, J. C.; Diego, J. A.; Mudarra, M.; Belana, J.; Diaz-Calleja, R.; Sanchis, M. J.; Jaimes, C. *Polymer* **1999**, *40*, 1181.
(6) Ito, E.; Tajima, K.; Kobayashi, Y. *Polymer* **1983**, *24*, 877.
(7) Buchner, S.; Wiswe, D.; Zachmann, H. G. *Polymer* **1988**, *30*, 480.
(8) Qian, R.; Shen, D.; Sun, F.; Wu, L. *Macromol. Chem.* **1996**, *197*, 1485.
(9) Lin, S.-B.; Koenig, J. L. *J. Polym. Sci. B: Polym. Phys.* **1982**, *20*, 2277.
(10) Stokr, J.; Schneider, B.; Doskocilova, D.; Lövy, J.; Sedlacek, P. *Polymer* **1982**, *23*, 714.
(11) Yang, X.; Long, F.; Shen, D.; Qian, R. *Polym. Commun.* **1991**, *32*, 125.
(12) Cole, K. C.; Guevremont, J.; Ajji, A.; Pellerin, E.; Dumoulin, M. M. *Polym. Mater.* **1996**, *75*, 63.
(13) Maxwell, A. S.; Ward, I. M.; Laupretre, F.; Monnerie, L. *Polymer* **1998**, *39*, 6835.
(14) Illers, K. H.; Breuer, H. J. *Colloid Sci.* **1963**, *18*, 1.
(15) Sacher, E. *J. Macromol. Sci. B* **1978**, *15*, 257.
(16) Chen, P.; Yee, A. F.; Goetz, J. M.; Schaefer, J. *Macromolecules* **1998**, *31*, 5371.
(17) Land, R.; Richards, R. E.; Ward, I. M. *Trans. Faraday Soc.* **1959**, *55*, 225.
(18) Reddish, W. *Trans. Faraday Soc.* **1950**, *46*, 459.
(19) Ward, I. M *Trans. Faraday Soc.* **1960**, *56*, 648.
(20) Armeniades, C. D. *J. Polym. Sci. B: Polym. Phys.* **1971**, *9*, 1345.
(21) Hedenqvist, M. S.; Bharadwaj, R.; Boyd, R. H. *Macromolecules* **1998**, *31*, 1556.
(22) Toxvaerd, S *J. Chem. Phys.* **1990**, *93*, 4290.
(23) (a) Haugk, M.; Elsner, J.; Frauenheim, T. *J. Phys.: Condens. Mater.* **1997**, *9*, 7305. (b) Elstner, M.; Porezag, D.; Jungnickel, G.; Frauenheim, Th.; Suhai, S.; Seifert, G. *Mater. Res. Soc. Symp. Proc.* **1998**, *491*, 131. (c) Elstner, M.; Porezag, D.; Seifert, G.; Frauenheim, Th.; Suhai, S. *Mater. Res. Soc. Symp. Proc.* **1999**, *538*, 541. (d) Cui, Q.; Elstner, M.; Kaxiras, E.; Frauenheim, T.; Karplus, M. *J. Phys. Chem. B* **2001**, *105*, 569.
(24) Frisch, J. G.; Trucks, W.; Schlegel, H. B.; Gill, P. M. W.; Johnson, B. G.; Robb, M. A.; Cheeseman, J. R.; Keith, T. A.; Petersson, G. A.; Montgomery, J. A.; Raghavachari, K.; Al-Laham, M. A.; Zakrzewski, V. G.; Ortiz, J. V.; Foresman, J. B.;. Cioslowski, J.; Stefanov, B. B.; Nanayakkara, A.; Challacombe, M.; Peng, C. Y.; Ayala, P. Y.; Chen, W.; Wong, M. W.; Andres, J. L.; Replogle, E. S.; Gomperts, R.; Martin, R. L.; Fox, D. J.; Binkley, J. S.; Defrees, D. J.; Baker, J.; Stewart, J. P.; Head-Gordon, M.; Gonzalez, C.; Pople, J. A. *Gaussian 94*; Gaussian, Inc.: Pittsburgh, PA, 1995.
(25) Møller, C.; Plesset, M. S. *Phys. Rev.* **1934**, *46*, 618.
(26) Lin, S. B.; Koenig, J. L. *J. Polym. Sci. B: Polym. Phys.* **1982**, *20*, 2277.
(27) Yazdanian, M.; Ward, I. M.; Brody, H. *Polymer* **1985**, *26*, 1779.

(28) Liu, J.; Koenig, J. L. *Anal. Chem.* **1987**, *59*, 2609.
(29) Yang, X.; Long, F.; Shen, D.; Qian, R. *Polymer* **1991**, *32*, 125.
(30) Rodriguez-Cabello, J. C.; Quintanilla, L.; Pastor, J. M. *J. Raman Spectrosc.* **1994**, *25*, 335.
(31) Ajii, A.; Guevremont, J.; Cole, K. C.; Dumoulin, M. M. *Polymer* **1996**, *37*, 3707.
(32) Schmidt-Rohr, K.; Hu, W.; Zumbulyadis, N. *Science* **1998**, *280*, 714.
(33) Martyna, G. J.; Tuckerman, M. E.; Klein, M. L. *J. Chem. Phys.* **1992**, *97*, 2635.
(34) Martyna, G. J.; Tobias, D. J.; Klein, M. L. *J. Chem. Phys.* **1994**, *101*, 4177.
(35) Martyna, G. J.; Tuckerman, M. E.; Tobias, D. J.; Klein, M. L. *Mol. Phys.* **1996**, *86*, 1117.
(36) Reddish, W. *Trans. Faraday Soc.* **1950**, *46*, 459.
(37) Zoller, P.; Bolli, P. *J. Macromol. Sci. Phys.* **1980**, *B18*, 555.
(38) Han, J.; Gee, R. H.; Boyd, R. H. *Macromolecules* **1994**, *27*, 7781.
(39) Jin, Y.; Boyd, R. H. *J. Chem. Phys.* **1998**, *108*, 9912.
(40) Fröhlich, H. *Theory of Dielectrics*, 2nd ed.; Oxford University Press: Oxford, U.K., 1958; Chapter 2.
(41) Saiz, E.; Hummel, J. P.; Flory. P. J.; Plasvic, M. *J. Phys. Chem.* **1981**, *85*, 3211.
(42) Smith. G. D.; Boyd, R. H. *Macromolecules* **1991**, *24*, 2731.
(43) Boyd, R. H.; Gee, R. H.; Han, J.; Jin, Y. *J. Chem. Phys.* **1994**, *101*, 788.
(44) Takeuchi, H.; Okazaki, K. *J. Chem. Phys.* **1990**, *92*, 5643.
(45) (a) Kohlrausch, R. *Ann. Phys.* **1847**, *12*, 393. (b) Williams, G.; Watts, D. C. *Trans. Faraday Soc.* **1970**, *66*, 80. (c) Williams, G.; Watts, D. C.; Dev, S. B.; North, A. *Trans. Faraday Soc.* **1971**, *67*, 1323.
(46) (a) Vogel, H. *Phys. Z.* **1921**, *22*, 645. (b) Fulcher, G. S. *J. Am. Chem. Soc.* **1925**, *8*, 339. (c) Fulcher, G. S. *J. Am. Chem. Soc.* **1925**, *8*, 789.
(47) From time-domain measurements that were the basis of the Fourier-transformed frequency data reported in ref 4 and were available to us. The frequency-domain representation shows definite composite structure that cannot be represented well by any of the standard phenomenological functions. The KWW function correspondingly does not fit the data especially accurately, but the low KKW β values found do express the extreme overall width of the process at low temperature.
(48) Gee, R. H.; Boyd, R. H. *J. Chem. Phys.* **1994**, *101*, 8028.
(49) Bharadwaj, R.; Boyd, R. H. *J. Chem. Phys.* **1999**, *110*, 10203.
(50) Roe, R. J. *Atomistic Modeling of Physical Properties*; Advances in Polymer Science Series; Monnerie, L., Suter, U., Eds.; Springer: New York, 1994.
(51) Pant. K.; Han, J.; Smith, G. D.; Boyd, R. H. *J. Chem. Phys.* **1993**, *99*, 597.
(52) Kim, E.-G.; Mattice, W. L. *J. Chem. Phys.* **1994**, *101*, 6242.
(53) (a) Takeuchi, H.; Roe, R. J. *J. Chem. Phys.* **1991**, *94*, 7448. (b) Takeuchi, H.; Roe, R. J. *J. Chem. Phys.* **1991**, *94*, 7458.
(54) Gee, R. H.; Boyd, R. H. *Comput. Theor. Polym. Sci.*, **1998**, *8*, 93.

MA0106797